Journal of Magnetic Resonance **140,** 218–227 (1999)
Article ID jmre.1999.1798, available online at http://www.idealibrary.com on IDEAL®

Frequency Dependence of EPR Signal-to-Noise

George A. Rinard, Richard W. Quine, James R. Harbridge, Ruitian Song, Gareth R. Eaton, and Sandra S. Eaton

Department of Engineering and Department of Chemistry and Biochemistry, University of Denver, Denver, Colorado 80208

Received March 1, 1999

Direct measurements of electron spin-echo signal and noise in well-characterized *X*-band and *S*-band spectrometers agree with predictions of frequency dependence based on first principles. For the particular spectrometers compared, the echo at 9.52 GHz was 9.5 times larger than the echo at 2.68 GHz, after scaling for differences in spectrometer gain. The calculated ratio was 7.6. This result contrasts with prior predictions that the frequency dependence would be much greater. © 1999 Academic Press

Key Words: **EPR; ESR; frequency dependence; *S/N*; noise.**

INTRODUCTION

Recently we rederived expressions for the frequency (ω) dependence of EPR signal-to-noise (S/N) (*1*), concluding that the well-known summary in the book by Poole (*2*) was in error by a factor of ω. The derivations are based on first principles, and the resulting equations for signal intensity give good agreement between experiment and theory for electron spin echo signal amplitudes and noise at *S* band (*3*). However, the long tradition of the Poole book results in appropriate skepticism of our revised predictions, and there exists a report from Kevan and co-workers (*4*) comparing S/N for their homebuilt *S*-band spectrometer (*5*) with a modern Bruker *X*-band spectrometer, which agrees (*4*) with the prediction in Poole's book. With this background we present a direct comparison of irradiated quartz echo amplitude and noise at *S* band and *X* band using well-characterized spectrometers and loop gap resonators.

FREQUENCY DEPENDENCE OF EPR SIGNAL INTENSITY

Continuous wave (CW) EPR signal intensity can be written as

$$V_S = \chi'' \eta Q \sqrt{P_A Z_0}, \qquad [1]$$

where V_S is the signal voltage at the end of the transmission line connected to the resonator, η (dimensionless) is the resonator filling factor, Q (dimensionless) is the loaded quality factor of the resonator, Z_0 is the characteristic impedance of the transmission line (in ohms), and P_A is the microwave power (in W) to the resonator produced by the external microwave source. The magnetic susceptibility of the sample, χ'' (dimensionless), is the imaginary component of the effective RF susceptibility.

For a Lorentzian line at resonance frequency ω, with width $\Delta\omega$ at half-height, substituting for the susceptibility in [1] yields

$$V_S = \frac{N\gamma^2\hbar^2}{4k_B T}\left(\frac{\omega}{\Delta\omega}\right)\eta Q_L\sqrt{Z_0 P}, \qquad [2]$$

where N is the number of spins per unit volume, k_B is Boltzmann's constant, T is the temperature of the sample, and we have introduced numerical coefficients for the case of $S = \frac{1}{2}$.

Experimental results that quantitatively satisfy Eq. [1] confirm the frequency dependence inherent in the terms of Eq. [1] (*3*). However, since many approximations must be made, and all measurements have inherent errors, measurement at more than one frequency is important to give confidence in the results. This is the reason for the treatment of both *S* band and *X* band in this paper.

We now examine relationships between some of the terms in Eq. [1], to make predictions of the functional dependence on microwave frequency. Consider first the effect of increasing the size of the resonator and sample while keeping both the sample concentration, N, and the filling factor, η, constant. The number of spins increases proportional to the increase in volume of sample. The increase in EPR signal is not directly proportional to this increase in number of spins, because the increase in size also affects Q through the change in resistance R and inductance L. However, if the resonator size and frequency are kept constant, and the sample size is increased, thus changing the filling factor η, the EPR signal would increase in proportion to the increase in volume of the sample. These statements assume that the sample is non-lossy and does not have a dielectric constant large enough to distort the RF B_1 distribution. Careful examination of the frequency dependence of each factor in Eq. [1] leads to the predictions for three cases that are summarized in Table 1: case 1—the size (linear dimensions) of the sample and resonator are constant, case 2—the size of the sample and resonator are scaled with $1/\omega$, and case 3—the size of the sample is constant and the size of the resonator is scaled with $1/\omega$.

1090-7807/99 $30.00

TABLE 1
Predicted Frequency Dependence of EPR Sensitivity When Resonator Resistance Dominates

		Case 1 (const. sample size, const. LGR size)	Case 2 (sample size $\propto 1/\omega$, LGR size $\propto 1/\omega$)	Case 3 (const. sample size, LGR size $\propto 1/\omega$)
1	L	1	ω^{-1}	ω^{-1}
2	R (resonator resistance)	$\omega^{1/2}$	$\omega^{1/2}$	$\omega^{1/2}$
3	Q	$\omega^{1/2}$	$\omega^{-1/2}$	$\omega^{-1/2}$
4	η	1	1	ω^{3}
5	EPR S/N at constant P	$\omega^{3/2}$	$\omega^{1/2}$	$\omega^{7/2}$
6	$B_1/\sqrt{P}$	$\omega^{-1/4}$	$\omega^{3/4}$	$\omega^{3/4}$
7	P to maintain constant B_1	$\omega^{1/2}$	$\omega^{-3/2}$	$\omega^{-3/2}$
8	EPR S/N at constant B_1	$\omega^{7/4}$	$\omega^{-1/4}$	$\omega^{11/4}$

If resonator size and sample size were kept constant, and the noise is determined by the resistive losses in the resonator, then the frequency dependence of each term in Eq. [2] leads to a prediction that S/N varies as $\omega^{7/4}$ in agreement with the analogous arguments put forth by Hoult and Richards (*6*) for certain NMR cases. The derivations of Eqs. [1] and [2] are expressed in terms related to CW experiments. It turns out to be more convenient for our comparison to derive expressions for echo signal intensity starting with the voltage induced in the resonator by the precessing spin magnetization. Following this we show the relationship between the expressions for spin echo and CW signal intensity.

CALCULATION OF TWO-PULSE ECHO INTENSITY

Precessing electron spin magnetization induces a current in the walls of the resonator. The task of calculating the resultant signal level encompasses four major steps. First, the relation between magnetization and signal in the resonator is calculated from first principles, using the inductance and resistance of the resonator. The relation between EPR lineshape and microwave B_1, as described by Bloom (*7*) and Mims (*8, 9*), was used to calculate the echo amplitude. Then the signal in the resonator was transformed to the other side of the resonator coupling device. Gains and losses from this point to the detector are used in the calculation of the predicted echo.

The electron spin echo voltage induced in the resonator is given by

$$V_S = N \frac{d\phi_0}{dt}, \qquad [3]$$

where N is the number of turns in the resonator and ϕ_0 is the magnetic flux produced by the spin magnetization, M_0. For all of the work presented here $N = 1$. Since the flux density produced by M_0 is $\mu_0 M_0$, ϕ_0 is given by

$$\phi_0 = \mu_0 \eta \mathbf{A} \cdot \mathbf{M}_0, \qquad [4]$$

where $\mathbf{A}$ is the cross-sectional area of the coil (resonator sample loop), η is the filling factor, and $\mu_0 = 4\pi 10^{-7}$. M_0 varies sinusoidally with the resonant frequency ω_0, and if the magnetization is fully turned to the xy plane by the microwave pulse, the peak voltage for a single-turn coil (a LGR) is

$$V_S = \mu_0 A \eta \omega_0 M_0, \qquad [5]$$

in agreement with (*10*).

The spin magnetization is given by

$$M_0 = N \frac{\gamma^2 \hbar^2 B_0}{4 k_B T} JT^{-1}\ \mathrm{m}^{-3}\ (=\mathrm{Am}^{-1}), \qquad [6]$$

so M/H is dimensionless, as required.

In this equation the static magnetic field $B_0 = \omega_0/\gamma$, k_B is Boltzmann's constant, and T is temperature in Kelvin. The magnetization of the irradiated fused quartz sample used for these studies was calculated using Eq. [6] based on the spin concentration, N, of 3×10^{17} spins/cm^3 ($\pm$10% uncertainty) (*16*), so $M_0 = 6 \times 10^{-4}\ JT^{-1}\ \mathrm{m}^{-3}$ at 293 K. There are 9.4×10^{15} spins in the sample. The same sample was used for both the *S*-band and *X*-band measurements.

In our measurements B_1 was of the same order as, or larger than, the linewidth, and the calculations (*7–9*) show that for this case the echo amplitude should approach the maximum possible for the magnetization, M_0. However, this calculation is only part of the story. The Bloom and Mims calculation is for spins on resonance. Off-resonant spins also contribute to the echo (or FID) (*11, 12*), and a $\pi/2$ pulse of strength B_1 will rotate ca. B_1 G of spectrum approximately 90° (*11*). Thus, the Bloom and Mims calculation somewhat underestimates the number of spins observed in an inhomogeneously broadened spectrum. One has to be sure that the same number of spins are observed at both frequencies and that the relaxation times are the same or are known and corrected for (*17*). The pulse repetition time was long enough (2 ms) that there was no T_1 effect. Since the

quartz EPR lineshape is determined by the distribution of g values (it is about 3 G wide at X band, and most of the spins are within a spectral width of about 1 G at S band), there could be concern whether the full spectrum was observed at both frequencies. To test for this we checked that the echo amplitude was independent of the pulse power by varying t_p while keeping the incident power adjusted for maximum echo. We also performed the very sensitive test for 90° pulses described in (*13*). Our observation of a clean null of the T echo in a $\pi/2$–τ–$\pi/2$–T–$\pi/2$–T echo sequence provided further assurance that all of the spins were turned in the measurements at both frequencies. Pulse widths, t_p, of 40 and 80 ns were used, corresponding to a ca. 4.5-G bandwidth excited by the second (more selective) pulse. The 40-ns $\pi/2$ pulse corresponded to B_1 of ca. 2.2 G. The 3-dB bandwidth at an overcoupled Q of 70 at S band was ca. 14 G and, for $Q = 118$ at X band, was ca. 29 G. Thus, by any of these criteria, the full spectrum was excited. These several approaches to the problem converge on the conclusion that it is reasonable in this case to use M_0 in Eq. [6] to calculate the echo amplitude.

Then, from Eq. [22] of Ref. (*14*), the output voltage of the resonator coupling structure, V_0, is given by

$$V_0 = \frac{\sqrt{\beta}}{1+\beta}\sqrt{\frac{Z_0}{R}}\,V_S, \qquad [7]$$

where R is the resistance of the resonator and Z_0 is the impedance of the transmission line (usually 50 Ω). The coupling parameter β is calculated from the overcoupled Q and the critically coupled Q, Q_H, by

$$\beta = \frac{2Q_H}{Q} - 1. \qquad [8]$$

Combining Eqs. [5] and [7] and the frequency dependence of M_0 from Eq. [6], V_0 can be written as

$$V_0 = k\,\frac{\sqrt{\beta}}{1+\beta}\sqrt{\frac{Z_0}{R}}\,\omega_0^2\eta A, \qquad [9]$$

where k includes the remaining terms from the above equations.

The ratio of the CW EPR intensity, Eq. [1], to the ESE intensity, Eq. [9], is $B_1/\Delta\omega$. This ratio is for the case in which $\beta = 1$, the ESE intensity is of the entire EPR signal, and we assume the CW EPR absorption signal is being detected. The ratio, then, increases with increase in B_1 and decreases the wider the line. The relationship between Eqs. [1] and [9] indicates that the frequency dependences of CW and spin echo signal intensity should be comparable, provided that in each case the characteristics of the spectrometer and resonator are taken into account.

For application to pulsed EPR, we chose not to calculate a filling factor to multiply the magnetization, but instead we calculated directly the echo amplitude as a function of B_1. The term $\mu_0 M_0 \eta A$ in Eq. [5] represents the magnetic flux that induces a voltage in the resonator,

$$\mu_0 M_0 \eta A = \int_{\text{sample}} \mathbf{M}\cdot\frac{B_1}{i}\,dV, \qquad [10]$$

where i is the current in the resonator. Thus, the use of the filling factor η is an approximation intended to avoid integrating over the sample. The approximation has to be defined for each case consistent with the experiment.

To calculate the ESE signal voltage directly, substitute [10] into [5],

$$V_S = \omega \int_{\text{sample}} \mathbf{M}\cdot\frac{B_1}{i}\,dV, \qquad [11]$$

and integrate over the sample volume. Since echo formation is a nonlinear function of B_1 (*7–9*), and B_1 is not uniform over the sample volume, we used the approximation that when B_1 is larger than the spectral width the echo is proportional to $\sin\theta_{pI}\sin^2(\theta_{pII}/2)$, which becomes $\sin^3\theta$ when the second pulse has twice the turning angle, θ, as the first one. Hence, the magnetization in the echo, which is the M to use in [11], is

$$M = M_0\sin^3\theta, \qquad [12]$$

where θ is calculated from the B_1 generated by the Ansoft Corporation High Frequency Structure Simulator (HFSS) software by assuming that at the center of the resonator the turning angle is 90°:

$$\theta = \frac{\pi}{2}\,\frac{B_{1\perp}}{B_{1\perp,0}}. \qquad [13]$$

$B_{1\perp,0}$ is the value of B_1 perpendicular to B_0 at the center of the resonator.

The signal voltage V_0 was calculated for the frequencies of the S-band and X-band experiments using Eq. [7]. As inputs the calculation requires the measured resonator Q, the coupling parameter, β, the resonator resistance, R, and the signal voltage in the resonator, V_S. Using Eqs. [11] and [12], V_S was calculated from the known magnetization of the sample and the B_1 distribution in the resonator calculated with HFSS software. The resistance, R, for the two resonators was estimated two ways. With the measured Q and frequency, one can estimate R

by calculating the inductance, L, which is given to a good approximation (*14*) by

$$L = \frac{\mu_0 \pi r^2}{z + 0.9r}, \quad [14]$$

where z is the length of the resonator and r is its radius. R can then be calculated using

$$R = \frac{\omega L}{2Q}. \quad [15]$$

The as-built dimensions of the *S*-band (2.68 GHz) LGR, 4.2-mm diameter and 10-mm length, yield $L = 1.46$ nH and $R = 0.027\ \Omega$. The second approach to calculating R is to use the formula for unit resistance (*15*),

$$R_S = \frac{1}{\sigma \delta(f)}, \quad [16]$$

where σ is the conductivity and $\delta(f)$ is the skin depth at frequency f,

$$\delta = \frac{1}{\sqrt{\mu_0 \pi f \sigma}}. \quad [17]$$

The effective length of the inner surface of the resonator is approximately $l_{\text{eff}} = 2\pi r + 2w/3$, where w is the width of the capacitive gap. This approximation is determined by integrating the power absorption around the loop and assuming linear variation of the current in the gap. Using 5.8×10^7 mho/m as the dc conductivity of copper, we calculate that the ac resistance at 2.68 GHz is

$$R_{\text{ac}} = \frac{R_S}{z} l_{\text{eff}} = 0.027\Omega. \quad [18]$$

Similar analysis of the 9.52-GHz split-ring resonator is a bit more uncertain, because the capacitive element does not have a flat surface. We visually estimate the effective width as 1.1 mm, which yields $R_{\text{ac}} = 0.073\ \Omega$. Calculating from the inductance of the loop, $R = 0.077\ \Omega$, which is in very good agreement.

The calculated values of V_0 were then multiplied by the net gain of each spectrometer, yielding 3.0 V at 2.68 GHz and 1.1 V at 9.52 GHz. The ratio of the calculated *X*-band to *S*-band echo amplitude, corrected for the difference in gains (Table 2), is 7.6. When we used Eq. [5] and assumed equal filling factors, the predicted ratio was 8.7 (Table 2). The predicted echo amplitude, based on the spin system and the overall system gain, assumes no decay due to relaxation. There is a dead time after the pulses during which one cannot observe the echo, but during which the echo amplitude decays. To account for the decay during the dead time, we measured the echo decay constant, T_m. The echo decay fits well to a single exponential, since the spin concentration in the sample is high enough that the decay is dominated by instantaneous diffusion (*16, 17*). Using the experimental T_m we calculated the echo amplitude at zero time.

CHARACTERIZATION OF THE *X*-BAND ELECTRON SPIN ECHO (ESE) SPECTROMETER

The previously described *X*-band ESE spectrometer (*18*) has been modified, with a new pulse programmer (*19*), a new 1-kW TWT (Applied Systems Engineering Model 117X), and a new signal detection path that is shown in Fig. 1. *S*-band measurements are described in detail in (*3*).

Crucial to the comparison of the spectrometers is a full characterization of the voltage gains and filter bandwidths of the signal detection paths. The EPR signal transfer function (the net effect of all gains and losses from the resonator to the display) was measured. For measurements of overall *X*-band spectrometer gain, microwave power was injected into a Bruker FlexLine unit at the connector to which the split-ring module is normally attached (where the EPR signal would enter). Consequently, the transfer function includes the signal loss in the coax from the resonator to the bridge. Powers were measured with an HP435B power meter. With the FlexLine unit attached to the ESE spectrometer, the 1.04-mW injected power was attenuated by a calibrated 40.3-dB attenuator. In addition, the power was attenuated a further 24 dB (total attenuation 64.4 dB) with a rotary vane attenuator before the detection system to avoid saturating the low-noise microwave amplifier. The detector PIN diode switch was held closed during the measurements of the transfer function, but it was controlled synchronously with microwave pulses in the normal way (*18*) during the echo amplitude and noise measurements. For the measurements of the transfer function, the microwave phase on the LO side of the DBM was adjusted for maximum signal and modulated $\pm$ 180° at 500 kHz. This approach yielded both positive and negative outputs from the IF port of the DBM, the average of which permitted elimination of any baseline offset. The dc voltage output (IF port) of the DBM was amplified and filtered as shown in Fig. 1 and the final voltage output was measured with a LeCroy 9310A digital oscilloscope with a 50-Ω input. Using the microwave power as described above, a gain of 11 on the amplifier after the DBM, and no filter, the square-wave-modulated signal measured on the LeCroy 9310A was 203.9 mV peak-to-peak. Thus, the average value was 102 mV into a 50-Ω load, which corresponds to 208 μW (-6.8 dBm). This corresponds to a net system gain of 57.4 dB (Table 2).

The manufacturer's test data on the MITEQ amplifier was available only for 9.0–9.2 GHz. A linear extrapolation to 9.5 GHz yields a gain of 45.2 dB. The amplifier after the DBM was

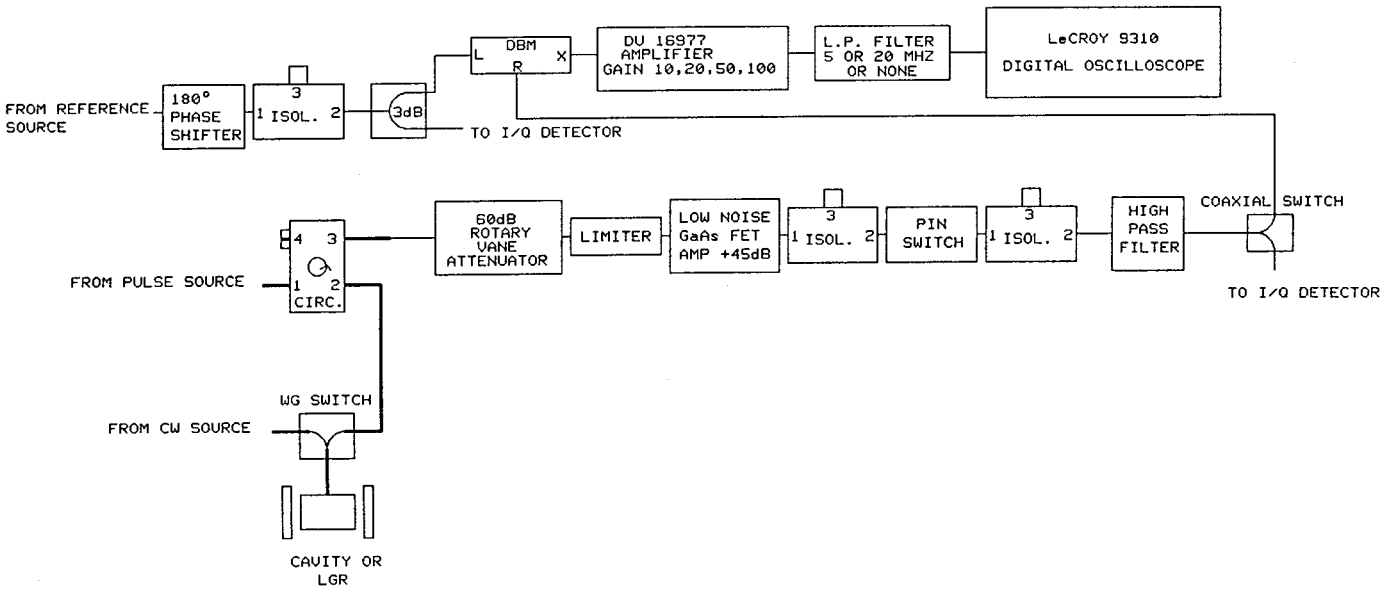

FIG. 1. *X*-band ESE spectrometer signal detection pathway. The portion of the spectrometer signal detection pathway that was used in the comparison study is presented. The components are interconnected with semirigid coaxial cables and sma connectors. The signal path, starting at the resonator is semirigid coax, waveguide (WR90 throughout), mechanical waveguide switch to select alternate paths, waveguide four-port circulator, 20-dB cross-guide coupler (to a pulse monitor crystal), rotary vane attenuator (for cases in which the echo is too strong), transition to sma and coaxial cable from this point on, limiter (Advanced Control Components ACLM-4533C-1K), isolator, low-noise microwave amplifier (MITEQ AMF-5S-9092-13, 44–45 dB gain, 1.14-dB NF), isolator, PIN diode switch (General Microwave DM864BH <2.6-dB nominal insertion loss), isolator, high-pass filter (Reactel 3HS-2000-S11, <0.5-dB insertion loss above 2 GHz), mechanical switch (Sage) to select alternate paths, double-balanced mixer (Western Microwave MJ45LX), amplifier. The amplifier used after the DBM is shown in detail in Fig. 2, and its properties are listed in Table 3.

used at gain = 11 (20.8 dB), so the estimated system gain was 66 dB. The 8.6-dB difference between the predicted 66-dB gain and the observed 57.4-dB gain is the loss inherent in the system. This included a 1.24-dB loss measured for the Flex-Line module. The mixer loss is not known separately but it was assumed to be the same as the 1.44 dB measured at *S* band. The switch and limiter and pieces of coax and connectors would add at least as much as at *S* band, so they should contribute at least 4 dB loss. These estimates give a total of about 7 dB loss. The agreement is within the errors of these estimates.

TABLE 2
Echo Amplitude and Standard Deviation Noise at *X* Band Relative to *S* Band

	2.68 GHz	9.52 GHz	*X*-band/*S*-band
Net system gain	84.0 dB	57.4 dB	1/21.4
Overcoupled Q	70	118	
Critically coupled Q	460	1163	
β	12	18.7	
Inductance, L (nH)	1.46	2.99	
Resistance, R (Ω)	0.027	0.077	
Observed echo corrected to time = 0	2.9 V	1.29 V	
Observed echo ratio normalized for gain			9.5
Predicted echo intensity (Eqs. [7], [11], and [12]) and ratio normalized for gain	3.0 V	1.1 V	7.6
Predicted echo ratio (Eq. [5]) assuming equal η			8.7
$\sqrt{\omega^5 Q}$	98.4	3038	30.9
SD noise after echo	80 mV	5.4 mV	
Amplifier noise figure	0.9 dB	1.14 dB*	
Effective noise bandwidth (MHz)	25.7	55.3	
SD noise normalized for gain and noise bandwidth	80	79	0.98

[a] The *X*-band amplifier noise figure was measured from 9.0 to 9.2 GHz.

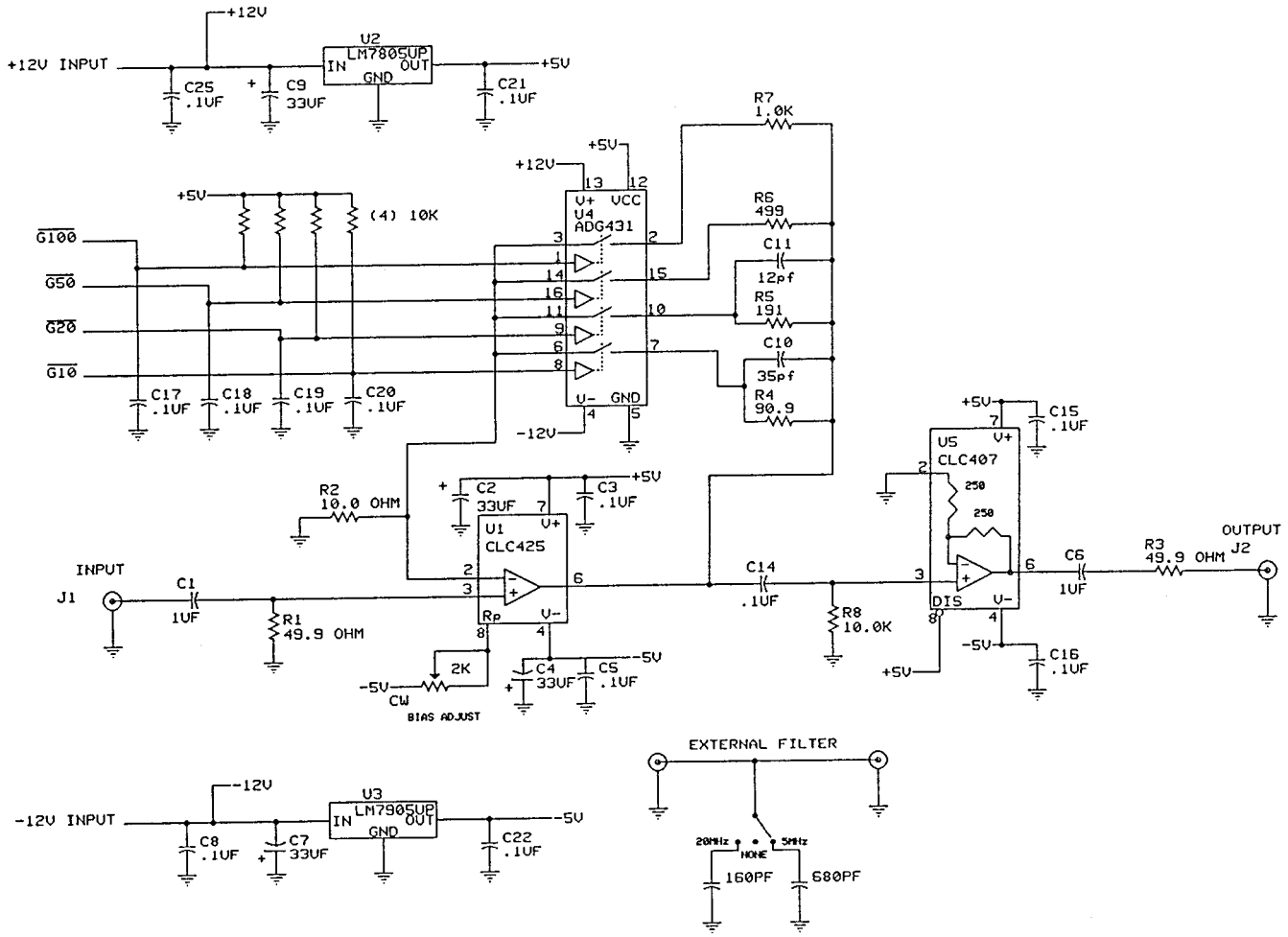

FIG. 2. ESE signal amplifier and filter. This amplifier provides selectable gains of 20, 26, 34, and 40 dB. The −3-dB bandwidths range from ca. 31 MHz at 20-dB gain to ca. 5.2 MHz at 40-dB gain. See tables in text for actual performance values. Gain is selected with an external switch that provides a ground to one of the gain selection lines G10, G20, G50, or G100. U1 is a low-noise (<0.9 nv/$\sqrt{\text{Hz}}$) integrated circuit op-amp (Comlinear-National Semiconductor P/N CLC425). The gain of this stage is established by the feedback resistors selected by analog switch U4. Capacitors C10 and C11 limit the bandwidth for the lower gains. Impedances are kept as low as possible to limit noise. A bias adjustment is provided to set the gain–bandwidth product of U1 and to provide stability margin. Amplifier U5 (Comlinear-National Semiconductor P/N CLC407) acts as a cable driver. It has a fixed gain of 6 dB to compensate for the loss in matching to the 50-Ω cable. Low-frequency cutoff is established at about 3.2 kHz by coupling capacitors C1 and C6. Voltage regulators U2 and U3 regulate ±12 V to ±5 V and provide power supply noise rejection. An external filter selection is provided to further limit the noise bandwidth. The nominal selections for the filter are 5 MHz, 20 MHz, or NONE. The saturation signal level is established by U5 and is ca. 2.5 V pp.

To make as direct a comparison of echo amplitudes between the *S*-band and *X*-band spectrometers as possible, we chose to use the Bruker ER4118-X-ms5 split-ring resonator for the *X*-band echo intensity study. The filling factor of this resonator is similar to that of the resonator used in the *S*-band experiments (*3*). HFSS software and dimensions obtained by inspection of the as-built resonator were used to calculate B_1 as a function of position in the resonator and in the irradiated quartz sample as outlined above, which is the same as previously reported for the *S*-band resonator (*3*).

The gain and bandwidth of the amplifier following the DBM in the *X*-band spectrometer (Fig. 2) directly impact the echo and noise measurements, so this amplifier was characterized in detail. In addition to standard bench tests of gain and 3-dB bandwidth (Table 3) we measured the effective noise bandwidth of the amplifier at various gain and filter settings, as described in (*3*). To check for the applicability of these measurements to the signal amplitude and noise in an actual electron spin echo (ESE) experiment, echo amplitude and standard deviation noise measurements were made in the configuration in which the *X*-band ESE spectrometer is commonly used. These values are in Table 4, where it is shown that the echo amplitude scaled for gain is constant within experimental error, and the standard deviation noise scaled for gain and filter noise bandwidth is also constant within experimental error. The use of effective noise bandwidth is essential for accurate comparison of noise in EPR spectrometers.

TABLE 3
Gain and Bandwidth of the Signal Amplifier following the *X*-Band DBM

Nominal gain	Gain at 1 MHz (dB)	Filter capacitor (pf)	Saturated output (V)	3-dB bandwidth (MHz)	Gain × bandwidth (MHz)	Effective noise bandwidth (MHz)
10	20.8 (11)[a]	None	2.6 V	31	341	55.3
		160		26		24.4
		680		8		10.2
20	26.2 (20.4)	None	2.6	21	428	26.4
50	34 (50)	None	2.5	12	600	14.3
100	39.4 (93)	None	2.6	5.2	484	7.7
		680		3.5		5.3

[a] Actual voltage gain in parentheses.

COMPARISON OF *X* BAND TO *S* BAND

The *X*-band measurements and calculations are compared with our prior *S*-band measurements [from Ref. (*3*)] in Table 2. The *X*-band echo amplitude was 953 mV under the following conditions: $Q = 118 \pm 3$; critically coupled $Q = 1163$; 40- and 80-ns pulses; $\tau = 496$ ns; 2-ms repetition period; voltage gain = 11, no filter. The SD noise after the echo was 5.3 mV. The echo decay function was measured to extrapolate the echo amplitude to time zero, resulting in the value of 1.29 V in Table 2. The *S*-band echo amplitude, corrected to zero time, was larger than the echo for the same sample at *X* band. The *S*-band spectrometer had 21.4 times the voltage gain of the *X*-band spectrometer, designed in anticipation of the sensitivity difference. After scaling the experimental echo amplitudes for the gain differences, the observed *X*-band echo amplitude is 9.5 times the *S*-band echo amplitude. This ratio is somewhat larger than the calculated ratio. Note that the calculated echo amplitude at *S* band is in better agreement with experiment than the value at *X* band (Table 2). One possible explanation is that the Bruker *X*-band resonator parameters were not known to us with the accuracy with which we measured the parameters of the homebuilt *S*-band resonator. We judge that the agreement between experiment and our predictions is better than the uncertainties in either value.

Because of the similarity of the resonators the relevant prediction of frequency dependence is very similar to case 1 in Table 1, but it is important to use the actual parameters of the resonators, as outlined above. Use of the $\omega^{7/4}$ dependence for case 1 of Table 1 would be erroneous, since that formula was derived with the assumption that the resonators were identical in size and that the frequency dependence came entirely from the conductivity of the materials of construction. However, were we to use the $\omega^{7/4}$ dependence we would calculate the ratio of the *X*-band to *S*-band echo as 9.2, which is in good

TABLE 4
Tests of the Gain of the Amplifier following the *X*-Band DBM[a]

Actual gain (from above)	Filter (pf)	Echo (V)	Echo scaled to gain = 50	SD noise after echo (mV)	Noise scaled to gain = 50, no filter	SD noise with 50-Ω load on input (mV)
11	None	0.330	1.50	5.3	12.3	5.4
	160			2.8	9.7	2.7
	680			1.9	10.2	1.8
20.4	None	0.608	1.49	5.6	10.1	5.7
	160			4.6		4.6
	680			3.1		3.2
50	None	1.45	1.45	9.6	9.6	9.9
	160			9.0		8.8
	680			6.8		6.9
93	None			13.7	10.0	13.8
	160			12.7		13.2
	680			10.7	9.4	11.1

[a] The performance happened to be measured using the Varian TE_{102} resonator with quartz Dewar insert, but the measured values do not depend on the resonator used. The scaled noise includes the square root of the measured effective noise bandwidth ratio.

agreement with our experimental results, because the resonators are fairly similar. Such a dependence would not fit the experiment if the resonators being compared were less similar.

The noise in the *S*-band spectrometer was found to agree within experimental error with the predictions for thermal noise of the sample plus noise added by attenuators and amplifiers in the signal detection and amplification path (*3*). The noise following the echo was measured at *X* band also. Scaling the noise for the differences in gain and for the square root of the effective noise bandwidths of the two spectrometers yielded essentially identical noise for the two spectrometers (Table 2). The right-hand column in Table 4 shows that the observed noise is the same whether the noise being amplified comes from a 50-Ω load at the input to the limiter in Fig. 1 or is the noise of the operating ESE system. These comparisons serve both as a confirmation of the measurements of the gains of the two spectrometers and also as a confirmation that in this *X*-band spectrometer, as in the *S*-band spectrometer, the measured standard deviation noise accompanying the signal is as expected for amplification of thermal noise.

COMPARISON WITH PRIOR RESULTS

Consider first the predictions when resonator noise dominates (Table 1). For the unlimited sample case, the dependence on $\omega^{1/2}$ agrees with the predictions of Abragam and Bleaney (*20*), Wilmshurst (*21*), and Fraenkel (*22*). For the limited sample case the dependence on $\omega^{7/2}$ agrees with the results of many others, including Feher (*23*), Abragam and Bleaney (*20*), and Fraenkel (*22*). The dependence of signal at constant power (*20, 22*) (unlimited sample, case 2) on $\omega^{1/2}$, of signal intensity for constant sample (case 3) at constant power (*20, 22–24*) on $\omega^{7/2}$, and of constant sample (*24*) (case 3) at constant B_1 on $\omega^{11/4}$ agrees with predictions in the references cited, among others. In the frequently cited discussion of $N_{\min}$ in (*2*), an additional factor of $1/\omega$ was included based on a set of assumptions concerning the frequency dependence of the relationship between incident microwave power in the waveguide outside a cavity and B_1 in the cavity. The relationships in Table 1 do not bear out this assumption.

The range of exponents in Table 1 indicates that one needs to consider carefully the experimental conditions in predicting frequency dependence of *S*/*N* for a particular situation. One also needs to consider practical realities. Scaling a resonator design over a wide frequency range may not be possible because of machining tolerances or because gaps become too small to prevent arcing for high-power and high-*Q* conditions. In addition, resonator dimensions may become so much smaller at higher frequencies that it is not possible to maintain a constant sample size. Thus the practical need for different resonators at different frequencies may prevent one from taking advantage of theoretically predicted advantages.

Based on early work by Hoult and co-workers (*6, 25–27, 43*), Andrew (*28*), and others (*29*) it is now generally agreed (*30*) that the *S*/*N* in MRI and spectroscopy in living systems follows a $\omega^{7/4}$ to ω^{1} frequency dependence. This is due to the fact that noise voltage due to resistance in the radiofrequency coil probe circuit is proportional to $\omega^{1/4}$, while noise due to losses in the patient's body is proportional to ω. At low frequencies where losses are small, the *S*/*N* varies as $\omega^{7/4}$ (Table 1, case 1). At higher frequencies, where the coil losses are less important, the *S*/*N* depends linearly on ω. Measurements at low frequency have confirmed the linear dependence of *S*/*N* on frequency in EPR (*31*) and NMR (*25, 32*).

If the filling factors of the resonators are about the same, and the detection systems of the two spectrometers are similar, the equations in Poole's book predict that the relative sensitivities would be proportional to (*2*, p. 550).

$$\frac{1}{\sqrt{\omega^5 Q}}. \qquad [19]$$

Since, when the resonator size is constant and the materials of construction are the same, $Q \propto \omega^{1/2}$, Eq. [19] predicts an $\omega^{11/4}$ dependence. Our derivation yields an $\omega^{7/4}$ dependence, when the sample size and resonator size are kept constant.

Other recent discussions in the literature comparing EPR *S*/*N* as a function of frequency have focused on frequencies above *X* band. Lebedev (*33*) pointed out that beyond the predictions of Poole (*2*), sensitivity will be affected by the anisotropy of the spectrum, because the signal increases in width as the frequency increases, and on the details of sample holders and sample loss at higher frequency. Prisner *et al.* (*34, 35*) state that the *S*/*N* of pulsed EPR should be proportional to

$$(S/N)_{\text{pulsed}} \propto \frac{\sqrt{Q\omega^3}}{\sqrt{V_c F \Delta f (kT)^3}}, \qquad [20]$$

where V_c is the cavity volume, F is the noise figure of the spectrometer, Δf is the detector bandwidth, and kT is the Boltzmann factor times temperature. The numerator of this expression is in agreement with our derivations, discussed above, and the denominator could, in principle, be constant in a frequency comparison, or each term could explicitly be accounted for. We do not agree with their statement that "for the same type of cavity" $Q \propto \omega^{-1}$. Consideration of the frequency dependence of the resistance of the materials of construction leads to a square root dependence on ω (*2*).

Weber *et al.* (*36*) state that the power emitted from a spin system in thermal equilibrium at room temperature after a $\pi/2$ pulse is

$$P_e \propto \frac{\omega^3 N^2 Q}{V_c}. \qquad [21]$$

Since the signal voltage is proportional to the square root of the power, this contains the same $\sqrt{\omega^3 Q}$ dependence as in our derived formulas.

These expressions from Prisner and Weber and co-workers (*34–36*), while not quantitatively tested in the cited papers, are consistent with the frequency dependence we obtained from first principles and which we tested with the measurements reported in this paper.

The predictions in Table 1 assume that Eq. [17] accurately represents the frequency dependence of conductivity of the materials of the resonator. This is the standard textbook formula. However, as frequency increases the conductivity is influenced increasingly by the surface properties rather than the bulk properties of the conductor. Machined, buffed, and plated surfaces are rough relative to skin depth at microwave frequencies and can contain inclusions from the finishing process. The machining and buffing processes result in work-hardening of the metal crystals, reducing their conductivity. These problems are discussed in (*37–40*). Some measurements, summarized in (*37–41*), reveal that the effective resistance at microwave frequencies is higher than the dc resistance, by as much as a factor of 2.5 or so, but typically that ratio is between 1.5 and 2, over the range 9–203 GHz. At 890 GHz the surface resistivity of evaporated gold was 2.2 times that expected from the dc resistivity (*42*). At frequencies below 9 GHz, the effective resistance approached the dc resistance. Only a very rough, scattered correlation with frequency and a stronger correlation with surface treatment and corrosion were observed (*42*). In general, plated specimens exhibited poor conductivity relative to theoretical. Recall that the resistance of the materials of which the resonator is built influences our predictions via the resonator Q, which is proportional to $\sqrt{\sigma}$. Since σ is the reciprocal of resistivity, a factor of 2 change in resistivity corresponds to a $\sqrt{2}$ decrease in Q and hence in EPR S/N. The conclusion from these observations is that the predictions of Eq. [1] may be as much as $\sqrt{2}$ optimistic for the improvement in signal intensity when the frequency in increased above *X* band, but that if the resonator losses dominate the noise, the S/N should still increase as predicted in Table 1. High-frequency (above *X* band) spectrometers will require improvements in sources, resonators, and detectors to achieve the theoretical improvement in S/N. The performance of low-frequency spectrometers should follow the predictions of Table 1 unless there are particularly resistive surfaces due to machining, plating, or corrosion.

CONCLUSIONS

The derived frequency dependence of S/N is consistent with our experimental data at X-band and S-band. In making such comparisons it is important to fully characterize the resonator and know the spectrometer transfer function.

ACKNOWLEDGMENTS

This research was supported in part by NSF Grant BIR-9316827 (G.R.E.) and by NIH Grant GM57577 (G.A.R.). We thank Dr. Ralph Weber for discussions concerning Ref. (*36*) and Professor Larry Kevan for discussion of Ref. (*4*).

REFERENCES

1. G. R. Eaton, S. S. Eaton, and G. A. Rinard, Frequency dependence of EPR sensitivity, *in* "Spatially Resolved Magnetic Resonance" (P. Blümler, B. Blümich, R. Botto, and E. Fukushima, Eds.), pp. 65–74, Wiley–VCH, Weinheim (1998).
2. C. P. Poole, Jr., "Electron Spin Resonance," Chap. 14, Wiley, New York (1967).
3. G. A. Rinard, R. W. Quine, R. Song, G. R. Eaton, and S. S. Eaton, Absolute EPR spin echo intensities, *J. Magn. Reson.,* accepted for publication.
4. M. Romanelli, V. Kurshev, and L. Kevan, Comparative analysis of pulsed electron spin resonance spectrometers at *X*-band and *S*-band, *Appl. Magn. Reson.* **7,** 427–441 (1994).
5. J. H. Hankiewicz, C. Stenland, and L. Kevan, Pulsed *S*-band electron spin resonance spectrometer, *Rev. Sci. Instrum.* **64,** 2850–2856 (1993).
6. D. I. Hoult and R. E. Richards, The signal-to-noise ratio of the nuclear magnetic resonance experiment, *J. Magn. Reson.* **24,** 71–85 (1976).
7. A. L. Bloom, Nuclear induction in inhomogeneous fields, *Phys. Rev.* **98,** 1105–1111 (1955).
8. W. B. Mims, Electron echo methods in spin resonance spectrometry, *Rev. Sci. Instrum.* **36,** 1472–1479 (1965).
9. W. B. Mims, Electron Spin Echoes, *in* "Electron Paramagnetic Resonance" (S. Geschwind, Ed.), Plenum, New York (1972).
10. N. Bloembergen and R. V. Pound, Radiation damping in magnetic resonance experiments, *Phys. Rev.* **95,** 8–12 (1954).
11. J. P. Hornak and J. H. Freed, Spectral rotation in pulsed ESR spectroscopy, *J. Magn. Reson.* **67,** 501–518 (1986).
12. E. Fukushima and S. B. W. Roeder, "Experimental Pulse NMR: A Nuts and Bolts Approach," Sect. II.A.2, Addison–Wesley, Reading, MA (1981).
13. W. H. Perman, M. A. Bernstein, and J. C. Sandstrom, A method for correctly setting the RF flip angle, *Magn. Reson. Med.* **9,** 16–24 (1989).
14. G. A. Rinard, R. W. Quine, S. S. Eaton, G. R. Eaton, and W. Froncisz, Relative benefits of overcoupled resonators vs. inherently low-*Q* resonators for pulsed magnetic resonance, *J. Magn. Reson. A* **108,** 71–81 (1994).
15. M. N. O. Sadiku, "Elements of Electromagnetics," 2nd ed., p. 472, Harcourt Brace College, Orlando, FL (1994).
16. S. S. Eaton and G. R. Eaton, Irradiated fused quartz standard sample for time domain EPR, *J. Magn. Reson. A* **102,** 354–356 (1993).
17. B. T. Ghim, S. S. Eaton, G. R. Eaton, R. W. Quine, G. A. Rinard, and S. Pfenninger, Magnetic field and frequency dependence of electron spin relaxation times of the *E′* center in irradiated vitreous silica, *J. Magn. Reson. A* **115,** 230–235 (1995).
18. R. W. Quine, G. R. Eaton, and S. S. Eaton, Pulsed EPR spectrometer, *Rev. Sci. Instrum.* **58,** 1709–1721 (1987).
19. R. W. Quine, "Programmable Timing Unit for Generating Multiple

Coherent Timing Signals," U.S. Patent 5,621,705, issued April 15 (1997).

20. A. Abragam and B. Bleaney, "Electron Paramagnetic Resonance of Transition Ions," Oxford Univ. Press, Oxford (1970).

21. T. M. Wilmshurst, "Electron Spin Resonance Spectrometers," Plenum, New York (1968).

22. G. K. Fraenkel, Paramagnetic resonance absorption, *in* "Technique of Organic Chemistry," Vol. I, Part IV: "Physical Methods of Organic Chemistry" (A. Weissberger, Ed.) 3rd ed., Chap. XLII, Interscience, New York (1960).

23. G. Feher, Sensitivity considerations in microwave paramagnetic resonance absorption techniques, *Bell System Tech. J.* **36,** 449–484 (1957).

24. Varian Spectrometer Manual 87-125-052, pp. 3–8.

25. D. I. Hoult, C.-N. Chen, and V. J. Sank, The field dependence of NMR imaging. II. Arguments concerning an optimal field strength, *Magn. Reson. Med.* **3,** 730–746 (1986).

26. D. I. Hoult and P. C. Lauterbur, The sensitivity of the zeugmatographic experiment involving human samples, *J. Magn. Reson.* **34,** 425–433 (1979).

27. D. I. Hoult, Sensitivity of the NMR experiment, *in* "Encyclopedia of NMR" (D. M. Grant and R. K. Harris, Eds.), Vol. 7, pp. 4256–4266 (1996).

28. E. R. Andrew, "Magnetic Resonance and Related Phenomena" (24th Ampere Congress, Poznan, 1988), pp. 45–51, Elsevier, Amsterdam (1989).

29. M. T. Vlaardingerbroek and J. A. den Boer, "Magnetic Resonance Imaging," Springer, New York (1996).

30. H. J. Halpern and M. K. Bowman, Low frequency EPR imaging, *in* "EPR Imaging and *in vivo* EPR" (G. R. Eaton, S. S. Eaton, and K. Ohno, Eds.), Chap. 6, CRC Press, Boca Raton, FL (1989).

31. L. G. Stoodley, The sensitivity of microwave electron spin resonance spectrometers for use with aqueous solutions, *J. Elect. Control* **14,** 531–546 (1963).

32. W. A. Edelstein, G. H. Glover, C. J. Hardy, and R. W. Redington, The intrinsic signal-to-noise ratio in NMR imaging, *Magn. Reson. Med.* **3,** 604–618 (1986).

33. Y. S. Lebedev, High-frequency continuous wave electron spin resonance, *in* "Modern Pulsed and Continuous-Wave Electron Spin Resonance" (L. Kevan and M. K. Bowman, Eds.), p. 372, Wiley, New York, (1990).

34. T. F. Prisner, M. Rohrer, and K. Möbius, Pulsed 95 GHz high-field EPR heterodyne spectrometer with high spectral and time resolution, *Appl. Magn. Reson.* **7,** 167–183 (1994).

35. T. F. Prisner, Pulsed high-frequency/high-field EPR. *Adv. Magn. Opt. Reson.* **20,** 245–299 (1997).

36. R. T. Weber, J. A. M. Disselhorst, L. J. Prevo, J. Schmidt, and W. Th. Wenkebach, Electron Spin echo at 95 GHz, *J. Magn. Reson.* **81,** 129–144 (1989).

37. R. S. Alger, "Electron Paramagnetic Resonance: Techniques and Applications," p. 133ff, Wiley–Interscience, New York (1968).

38. F. A. Benson, Attenuation of rectangular waveguides, *in* "Millimetre and Submillimetre Waves" (F. A. Benson, Ed.), Iliffe Books, London (1969).

39. P. F. Goldsmith, Quasi-optical techniques at millimeter and submillimeter wavelengths, *Infrared Millimeter Waves* **6,** 277–342 (1982).

40. P. F. Goldsmith, "Quasioptical Systems: Gaussian Beam Quasioptical Propagation and Applications," pp. 119ff, 303ff, IEEE Press, New York (1998).

41. F. Losee, "RF Systems, Components, and Circuits Handbook," p. 345, Artech House, Boston (1997).

42. R. J. Batt, G. D. Jones, and D. J. Harris, The measurement of the surface resistivity of evaporated gold at 890 GHz, *IEEE Trans. Microwave Theory Techniques* **MTT-25,** 488–491 (1977).

43. C.-N. Chen and D. I. Hoult, "Biomedical Magnetic Resonance Technology," Adam Hilger, Bristol (1989).